

Maxwell-Boltzmann Distribution of M^{3+} - F^- Interstitial Pairs in Fluorite-Type Lattices*

RICHARD H. HEIST† AND FRANCIS K. FONG

Department of Chemistry, Purdue University, Lafayette, Indiana 47907

(Received 17 November 1969)

Maxwell-Boltzmann distribution curves for M^{3+} - F^- interstitials in fluorite-type lattices have been calculated and compared with spectroscopic data. The dominant sites, in the order of their relative importance for low concentrations and $T < 700$ K, are the $C_{4v}(1,0,0)$, $C_s(2,1,0)$, $C_{3v}(1,1,1)$, $C_s(1,2,2)$, $C_s(1,1,3)$, and $C_s(2,3,0)$ sites. The dominant presence of the third-nearest-neighbor monoclinic $C_s(2,1,0)$ pair, which has not been reported previously, is predicted by our calculations. In view of this result, the electron spin resonance data on U^{3+} in CaF_2 reported by Mahlab, Volterra, Low, and Yariv, which these authors interpreted in terms of the fifth-nearest-neighbor site, have been shown to arise actually from the prominent presence of the third-nearest-neighbor $C_s(2,1,0)$ site.

I. INTRODUCTION

IN the investigation of charge compensation phenomena in ionic crystal lattices, there are two outstanding examples. The first and older example is the charge compensation by metal ion vacancies of impurity divalent ions in alkali halides. The second example, which has recently attracted a large number of investigations, is the charge compensation by fluoride interstitials of trivalent cations in alkaline earth fluorides. Recent papers¹⁻⁴ from this laboratory have shown that in (alkali halide): M^{2+} systems, the impurity divalent ions exist in a multiplicity of site symmetries which can be readily explained in terms of a Maxwell-Boltzmann distribution in the interaction energies between the divalent ions and the compensation defect vacancies. Such a treatment is valid only at sufficiently low temperature and concentration when the canonical configuration partition function becomes expressible as a product of "molecular" partition functions.² It became obvious that the procedure employed in the case of the (alkali halide): M^{2+} systems can be readily extended to the (alkaline-earth halide): M^{3+} systems in which compensation is characterized by F^- interstitials.

The initial difficulty which confronts us in our present effort is the lack of a good knowledge of the interaction energies between the trivalent ions and the F^- interstitials. While the interactions between more distant M^{3+} - F^- interstitial pairs can be safely assumed to be nearly Coulombic in nature, interactions between the closer pairs, particularly the nearest and the next nearest neighbors, are virtually unknown. Unlike the alkali halide systems, for which both the calculated⁵

and experimentally observed values⁶ for the nearest neighbor and next nearest neighbors are well documented, corresponding values for the (alkaline earth halide): M^{3+} systems have yet to be firmly established. Nevertheless, there is such an abundance of experimental data available that we have been able to find sufficient clues for a reasonably satisfactory application of the distribution theory outlined earlier² to the M^{3+} - F^- interstitial compensation problem.

In the following sections of this paper, we shall first construct our distribution calculations from known literature results. We shall then employ these calculated distributions in a systematization of the numerous spectroscopic observations concerning the site symmetries of the trivalent cation in the fluorite-type lattice. A surprising result of our calculations is the prediction of the dominant present of the third-nearest-neighbor pair which has not been reported previously. In view of this prediction, we shall show that the interesting electron spin resonance (ESR) spectroscopic observation of what was thought to be an "orthorhombic" U^{3+} site is actually due to the predicted presence of the third-nearest-neighbor monoclinic site.

II. OBSERVED SITE SYMMETRIES OF TRIVALENT CATIONS IN FLUORITE-TYPE CRYSTALS

A profusion of different site symmetries have been reported for the trivalent cation in fluorite-type crystals. In practically all the ESR investigations, the predominant sites reported were either cubic⁷⁻¹¹ or tetragonal.^{7,8,10-13} In recent years, numerous authors reported the observation of two different trigonal sites in CaF_2 ,

* This work was supported under the institutional Advanced Research Projects Agency Grant No. SD102.

† This paper represents part of the work submitted by R. H. Heist to the Graduate School of Purdue University in partial fulfillment of the requirement for the degree of Doctor of Philosophy.

¹ F. K. Fong and E. Y. Wong, *Phys. Rev.* **162**, 348 (1967).

² F. K. Fong, *Phys. Rev.* **187**, 1099 (1969).

³ F. K. Fong, R. H. Heist, C. R. Chilver, J. C. Bellows, and R. L. Ford, *J. Luminescence* (to be published).

⁴ F. K. Fong, *Phys. Rev.* (to be published).

⁵ F. Bassani and F. G. Fumi, *Nuovo Cimento* **11**, 274 (1954); M. P. Tosi and G. Airoldi, *ibid.* **8**, 584 (1958).

⁶ G. D. Watkins, *Phys. Rev.* **113**, 79 (1959); **113**, 91 (1959).

⁷ U. Ranon and W. Low, *Phys. Rev.* **132**, 1609 (1963).

⁸ C. W. Rector, B. C. Pandey, and H. W. Moos, *J. Chem. Phys.* **45**, 171 (1966).

⁹ R. W. Bierig and M. J. Weber, *Phys. Rev.* **132**, 164 (1963).

¹⁰ U. Ranon and A. Yariv, *Phys. Letters* **9**, 17 (1964).

¹¹ J. Sierro, *Phys. Letters* **4**, 178 (1963).

¹² M. J. Weber and R. W. Bierig, *Phys. Rev.* **134**, A1492 (1964).

¹³ V. M. Vinokurov, M. M. Zaripov, Yu. T. Pol'skii, V. G. Stepanov, G. K. Chirkin, and L. Ya. Shekun, *Fiz. Tverd. Tela* **4**, 2238 (1962); **5**, 599 (1963) [English transl.: *Soviet Phys.—Solid State* **4**, 1637 (1963); **5**, 436 (1963)].

TABLE I. ESR observations of trivalent rare earth ions in alkaline earth fluorides. Listed properties include the observed site symmetry, the proposed compensation, g values, and crystal-field parameters. Results tabulated are characteristic of work since 1963.

Host crystal	Rare-earth ion	Site symmetry observed	Proposed compensation	Characterization		Crystal-field parameters		Reference
				g values		b_2^0 (10^4 cm $^{-1}$)	b_4^0 (10^4 cm $^{-1}$)	
CaF ₂	Gd ³⁺ (f^7)	O_h	Nonlocal				46.6±0.3	11
		C_{4v}	n.n. F _i ^{-a}			1488±5.0	23.0±1.5	
		C_{3v}	O ²⁻			1666±6.0	39.3±1.5	
		C_{3v}	OH ⁻			407±4.0	-21.2±0.5	
CaF ₂	Gd ³⁺ (f^7)	C_{4v}	n.n. F _i ^{-a}	$g_{11}=1.992±0.001$	$g_1=1.992±0.001$			13
CaF ₂	Er ³⁺ (f^{11})	O_h (30) ^b	Nonlocal	$g=6.78±0.01$				7
		C_{4v} (30)		$g_{11}=7.78±0.02$	$g_1=6.254±0.005$			
		C_{4v} (10)	n.n. F _i ^{-a}	$g_{11}=1.746±0.002$	$g_1=9.16±0.01$			
		C_{3v} (1)	OH ⁻	$g_{11}=3.3±0.01$	$g_1=8.54±0.02$			
CaF ₂	Er ³⁺ (f^{11})	C_{3v} (9)	O ²⁻	$g_{11}=2.206±0.007$	$g_1=8.843±0.01$			8
		O_h (15) ^b	Nonlocal	$g=6.78±0.02$				
		C_{4v} (20)	n.n. F _i ^{-a}	$g_{11}=7.78±0.02$	$g_1=6.25±0.01$			
		C_{3v} (1)	n.n.n. F _i ^{-c,d}	$g_1=3.29±0.01$	$g_1=8.55±0.02$			
CaF ₂	Yb ³⁺ (f^{13})	O_h	Nonlocal	$g=3.441±0.003$				10
		C_{4v}	n.n. F _i ^{-a}	$g_{11}=2.42±0.004$	$g_1=3.802±0.003$			
		C_{3v}	O ²⁻	$g_{11}=1.323±0.001$	$g_1=4.389±0.004$			
		C_{3v}	OH ⁻	$g_{11}=1.421±0.001$	$g_1=4.389±0.004$			
CaF ₂	Yb ³⁺ (f^{13})	O_h	Nonlocal	$g=3.441±0.004$				12
CaF ₂	Yb ³⁺ (f^{13})	C_{4v}	n.n. F _i ^{-a}	$g_{11}=2.423±0.001$	$g_1=3.878±0.001$			14
		C_{3v}	O ²⁻	$g_{11}=1.323±0.002$	$g_1=4.389±0.005$			
CaF ₂	U ³⁺ (f^3)	O_h	Nonlocal					17
		C_{4v}	n.n. F _i ^{-a}	$g_x=1.38±0.01$	$g_y=2.85±0.02$			
		Orthorhombic	5th n.n. F _i ^{-e}	$g_z=2.94±0.01$				
SrF ₂	Gd ³⁺ (f^7)	O_h	Nonlocal				41.0±0.5	11
		C_{4v}	n.n. F _i ^{-a}			1123±8.0	19.7±3.0	
		C_{3v}	O ²⁻			1816±8.0	30.2±4.0	
		C_{3v}				138±8.0	40.8±0.4	
SrF ₂	Yb ³⁺ (f^{13})	O_h	Nonlocal	$g=3.438±0.002$				10
		C_{3v}	O ²⁻	$g_{11}=1.345±0.002$	$g_1=4.420±0.004$			
		C_{3v}	n.n.n. F _i ^{-c}	$g_{11}=2.804±0.003$	$g_1=3.743±0.009$			
BaF ₂	Gd ³⁺ (f^7)	O_h	Nonlocal				36.2±0.3	11
BaF ₂	Yb ³⁺ (f^{13})	C_{3v}	O ²⁻	$g_{11}=1.334±0.002$	$g_1=4.405±0.005$	136±8.0	35.9±0.4	10
		C_{3v}	n.n.n. F _i ^{-c}	$g_{11}=2.763±0.003$	$g_1=3.768±0.003$			

^a Nearest-neighbor interstitial fluoride ion.

^b Relative intensities of ESR spectral lines are given in parentheses.

^c Next-nearest-neighbor interstitial fluoride ion.

^d The authors (Ref. 8) made no site origin assignment to their observation of the trigonal site symmetry. Earlier attribution (Ref. 7) of this site to second-nearest-neighbor OH⁻ compensation is unlikely (see text). The crystals were grown (Ref. 8) under a F₂ atmosphere to exclude O²⁻ contamination. In the absence of O²⁻ ions, the most probable trigonal compensation arises from the n.n.n. F⁻ interstitial compensation.

^e Fifth-nearest-neighbor interstitial fluoride ion.

one of which has been attributed^{7,9-11,13,14} to the incorporation of O²⁻ ions in the F⁻ sublattice while the second has been assigned to OH⁻ interstitial compensation.^{7,15,16} A summary of pertinent ESR observations for the various paramagnetic trivalent rare earth ions in CaF₂, SrF₂, and BaF₂ crystals is given in Table I.

Current interpretations of the results listed in Table I ascribe the cubic sites to M³⁺ ions in non-local compensation beyond any observable influence of the associated F⁻ interstitials. The tetragonal sites are usually attributed^{7,8,10-12,17} to nearest neighbor M³⁺-F⁻

interstitial pairs. The introduction of O²⁻ ions in the F⁻ sublattice will give rise to a trigonal site^{7,10,11,14} as the M³⁺-O²⁻ pair will be directed along the [111] axis. The postulate^{7,15,16} that an interstitial OH⁻ ion gives rise to the second observed trigonal site is not easily understood since the OH⁻ ion can be expected to prefer the nearest-neighbor tetragonal site on grounds of a greater stabilization energy as in the case of the F⁻ compensation. There are two reported tetragonal sites in CaF₂:Er³⁺, the first characterized by $g_{11}=7.78±0.02$ and $g_1=6.25±0.01$,^{7,8} and the second by $g_{11}=1.746±0.002$ and $g_1=9.16±0.01$.⁷ Both sites were observed by Ranon and Low,⁷ whereas Rector, Pandey, and Moos (RPM), in a recent investigation,⁸ reported only the first tetragonal site in crystals which have been grown under a fluorine atmosphere. Since the presence of F₂

¹⁴ S. D. McLaughlan and R. C. Newman, Phys. Letters 19, 552 (1965).

¹⁵ W. Low and U. Ranon, in *Paramagnetic Resonance*, edited by W. Low (Academic Press Inc., New York, 1963), p. 167.

¹⁶ J. Sierro, J. Chem. Phys. 34, 2183 (1961).

¹⁷ E. Mahlab, V. Volterra, W. Low, and A. Yariv, Phys. Rev. 131, 920 (1963).

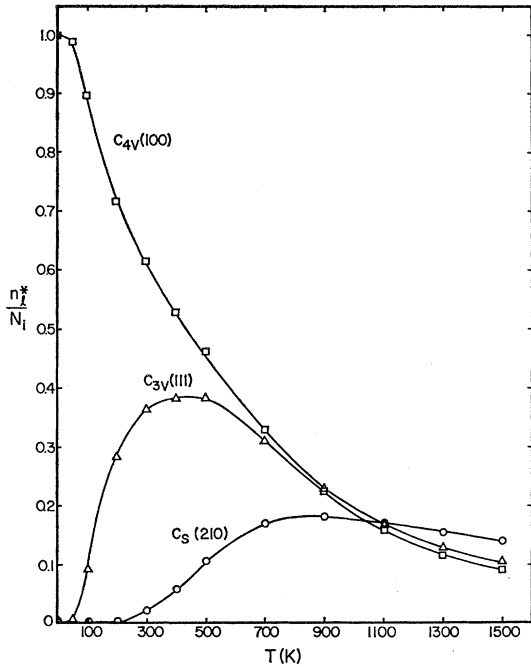


FIG. 1. The calculated probabilities, n_i^*/N_i , of finding the $C_{4v}(1,0,0)$, $C_{3v}(1,1,1)$, and $C_s(2,1,0)$ sites assuming the homogeneous dielectric shielding model for ϵ_l ($l \geq 2$) with $\epsilon_1 = -0.48$ eV. The prominence of the trigonal sites does not agree with the experimental tetragonal to trigonal intensity ratio observed by RPM (Ref. 8) (see Table I).

atmosphere during crystal growth is expected to exclude the possibility of O^{2-} or OH^- compensation, the assignment of the first tetragonal site to the nearest neighbor M^{3+} - F^- interstitial pair appears to be reasonable. In view of this, we believe that the RPM results are more representative of the $CaF_2:M^{3+}$ system in which only the F^- interstitials are responsible for the compensation. The results of investigations^{7,16,18} in which additional compensation is achieved by impurity ions such as Na^+ ,¹⁸ O^{2-} ,^{7,16} and OH^- ^{7,16} are interesting. However, the understanding of the "pure" system is essential before a meaningful discussion of the effect of additional compensation mechanisms can be attempted.

III. DISTRIBUTION OF M^{3+} SITE SYMMETRIES IN $CaF_2:M^{3+}$ SYSTEM

Since the most familiar fluorite-type host is CaF_2 , we shall concentrate on it as an example. The cation sublattice is face-centered cubic. When a M^{3+} ion enters the cation sublattice substitutionally, a F^- interstitial is created so that charge neutrality is maintained. Under the conditions specified in the earlier work² on the $KCl:M^{2+}$ system, we can, as a first approximation, assume that each M^{3+} ion is paired with a F^- interstitial, and that the energy of association varies as R_l^{-1} , where R_l is the distance of separation and l denotes an inter-

stitial in the l th nearest-neighbor (n.n.) position. Since the F^- interstitial can only occupy discrete positions, R_l can only take on discrete values, with the consequence that the Coulombic energy of association is also discrete:

$$\epsilon_l = -e^2/\epsilon R_l,$$

where $\epsilon = 6.7$ for CaF_2 . If the point occupied by the interstitial F^- in a given pair is denoted by (i, j, k) , $(i+j+k)$ must be odd. The value for R_l is simply $(i^2 + j^2 + k^2)^{1/2}a$, where $a = 2.718 \text{ \AA}$ is half the distance between two neighboring Ca^{2+} ions. R_l can be written as $(2l-1)^{1/2}a$, where $l = 1, 2, 3, \dots$, except that for $l = 4, 8, 12, 16, \dots$, $g_l = 0$. The various site symmetries (and corresponding values of the number of distinguishable but equivalent lattice points, g_l , in parenthesis) are: C_{4v} (6) when $i \neq 0, j = k = 0$; C_s (24) when $i \neq j, k = 0$ and $i, j \neq 0$; C_1 (48) when all i, j, k are unequal and unequal to zero; and C_{3v} (8) when $i = j = k \neq 0$. At $l = 5, 9, 13, 17, 21, 25, 29$, and 33 more than one site symmetry can occur.

The energy of pairing can now be written

$$\begin{aligned} \epsilon_1 &= -0.48 \text{ eV}, \\ \epsilon_l &= -e^2/[\epsilon(2l-1)^{1/2}a], \end{aligned} \quad (1)$$

where $l = 2, 3, \dots$. The value $\epsilon_1 = -0.48$ eV is assumed to be the same as that found for the association of the nearest-neighbor Y^{3+} - F^- interstitial pair.¹⁹ The pairing energies for $l > 1$ are estimated by assuming the simple homogeneous dielectric shielding model. In the $KCl:M^{2+}$ system, this has been seen to be a fairly good approximation.² Its validity in the present case will be tested shortly.

Assuming the conditions for the canonical ensemble, at sufficiently low temperatures and concentrations,² we write for the distribution numbers n_i^* associated with the energy level ϵ_l :

$$n_i^* = \frac{N_i g_l e^{-\epsilon_l/kT}}{\sum_{l'} g_{l'} e^{-\epsilon_{l'}/kT}} = N_i q_p^{-1} g_l e^{-\epsilon_l/kT}, \quad (2)$$

where the crystal contains N_i impurity atoms/cm³, and q_p is the molecular partition function for the pair formation. Equation (2) holds subject to the restrictive conditions

$$E_p = \sum_l n_l^* \epsilon_l$$

and

$$N_i = \sum_l n_l^*, \quad (3)$$

where E_p is the total energy of the crystal due to pairing. The calculated values of (n_i^*/N_i) are plotted against T in Fig. 1 for the first three bound states.

¹⁹ B. R. Rossing, Ph.D. thesis, Massachusetts Institute of Technology, Boston, 1966 (unpublished).

¹⁸ J. Kirton and S. D. McLaughlan, Phys. Rev. **155**, 274 (1967).

It is immediately obvious that the results shown in Fig. 1 do not fit the experimental results reported by RPM. Since we have concluded in Sec. II that their results appear to be the most relevant to our present discussion due to the precautions taken in their crystal preparation, we shall proceed to vary ϵ_2 in order to fit our calculations to their observations. In this approach, we assume the simple homogeneous dielectric shielding model for ϵ_l where $l \geq 3$. The experimental result crucial to our calculation is the ratio 20:1 corresponding to the relative ESR intensities of the tetragonal sites to the trigonal sites. In the language of the F^- interstitial compensation theory, we have $n_1/n_2=20$. Taking $\epsilon_1 = -0.48$ eV as before, and assuming Coulombic values for $\epsilon_l (l \geq 3)$, we solve graphically for ϵ_2 and T from the equations:

$$n_1^*(\epsilon_2, T) = 6N_i q_p^{-1}(\epsilon_2, T) e^{0.48/kT}$$

and

$$n_2^*(\epsilon_2, T) = 0.05n_1^*(\epsilon_2, T) = 8N_i q_p^{-1}(\epsilon_2, T) e^{-\epsilon_2/kT}$$

obtaining $\epsilon_2 = -0.30$ eV and $T = 630$ K. We note that the value of ϵ_2 is roughly 30% lower than the corresponding Coulombic value -0.46 eV, which would accordingly lower the probability of finding the trigonal sites in our distribution calculation. The resulting distribution curves for the first three bound states are shown in Fig. 2. In Fig. 3, the next four higher bound states are shown. In our calculations, q_p is summed

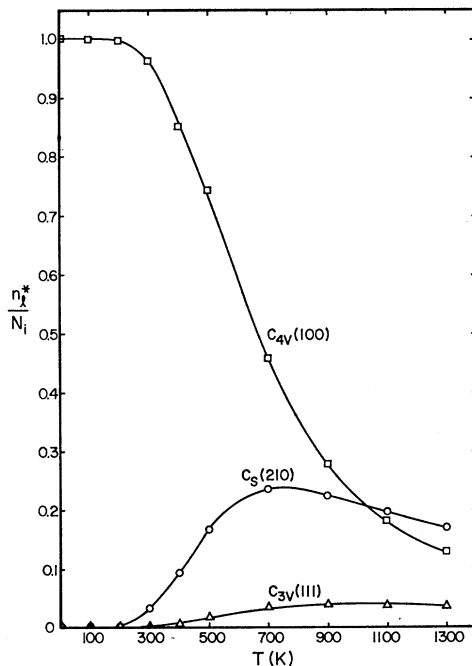


FIG. 2. The calculated probabilities, n_i^*/N_i , of finding the $C_{4v}(1,0,0)$, $C_{3v}(1,1,1)$, and $C_s(2,1,0)$ sites assuming the homogeneous dielectric shielding model for $\epsilon_l (l \geq 3)$ with $\epsilon_1 = -0.48$ eV and $\epsilon_2 = -0.30$ eV. The calculations are made for the best parameter fit of the RPM data (Ref. 8).

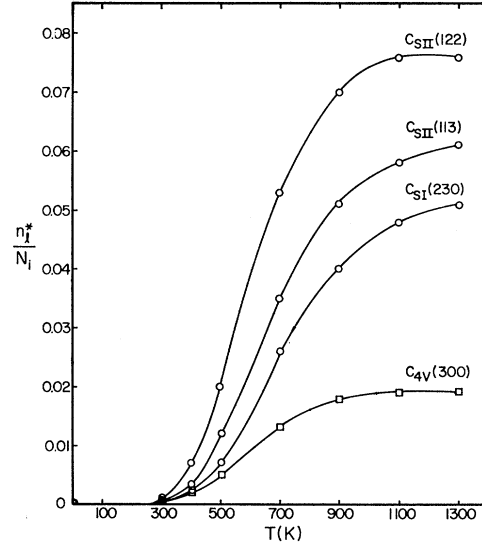


FIG. 3. The calculated probabilities, n_i^*/N_i , of finding the $C_s(1,2,2)$, $C_s(1,1,3)$, $C_s(2,3,0)$, and $C_{4v}(3,0,0)$ sites assuming the homogeneous dielectric shielding model for $\epsilon_l (l \geq 3)$ with $\epsilon_1 = -0.48$ eV and $\epsilon_2 = -0.30$ eV.

over $l=1, 2, \dots, 21$ for $T=0, 100, 200, 300, 400, 500, 700, 900, 1100,$ and 1300 K. When $\epsilon_l \gg kT$, only the ground level ϵ_1 is populated, and $q_p = g_1 e^{-\epsilon_1/kT}$ leading to the result that $n_1^* = N_i$, i.e., all the M^{3+} ions and F^- interstitials are associated as the nearest-neighbor pairs. As T increases, the excited levels become populated. The partition function must now be summed over successively increasing values of l to obtain accurate results. At $T < 700$ K the value for q_p does not change significantly when the sum is carried beyond $l=16$, whereas at higher temperatures, the terms in q_p beyond $l=16$ become increasingly significant, and q_p apparently does not converge readily. The causes for this difficulty have been discussed previously.² Thus, in using the molecular partition function approach, we have meaningful values of q_p only at temperatures less than 700 K. At higher temperatures, population of states corresponding to large separations leads to configuration energies which are mathematically intractable.² Calculations of q_p at these temperatures are thus subject to serious errors. Nevertheless, even at 1300 K, the largest terms in q_p are still those characterized by the smallest l values, i.e., those corresponding to the low-lying bound states.

IV. THIRD-NEAREST-NEIGHBOR $C_s(2,1,0)$ M^{3+} - F^- INTERSTITIAL PAIR

An inspection of Fig. 2 indicates that for the temperature range in which the calculations of q_p are valid, practically all the trivalent impurity cations are in close association up to the third nearest neighbor with the associated F^- interstitials. If this result is true, how do we account for the frequently reported cubic sites? Since the results shown in Fig. 2 have been obtained

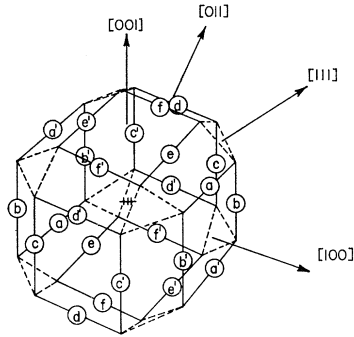


FIG. 4. The 12 magnetically distinguishable $C_s(2,1,0)$ M^{3+} - F^{-} interstitial sites; $a, a', b, b', c, c', d, d', e, e', f, f'$.

through a fit of the RPM's observed ratio of $n_1^*:n_2^* = 20:1$, many of the so-called cubic sites must correspond to the third-nearest-neighbor $C_s(2,1,0)$ M^{3+} - F^{-} interstitial pair, the significant presence of which is a dominant feature of the distribution data shown in Fig. 2. The situation with which we are faced is almost identical to that encountered in the case of the (alkali halide): M^{2+} system.^{2,4} It was shown by an idealized statistical calculation that the third-nearest-neighbor $C_s(2,1,1)$ site should be the second most probable site.² However, there was no existing report of the experimental observation of such a third-nearest-neighbor site. Instead, a large signal attributed to cubic sites was reported by the ESR work of Watkins⁶ for the $KCl:Mn^{2+}$ and $NaCl:Mn^{2+}$ systems. Since the prediction of the dominant presence of the $C_s(2,1,1)$ site, however, we have firmly established⁴ the dominant presence of the third nearest neighbor M^{2+} - K^+ vacancy pair in the $KCl:Sm^{2+}$ system by means of Zeeman anisotropy fluorescence spectroscopy. Since in the present investigation the interactions between the closer pairs are not as well established as those in the (alkali halide): M^{2+} systems, the positive identification of the third-nearest-neighbors $C_s(2,1,0)$ pair is all the more desirable if our distribution calculations are to be given any credibility.

In our search for the $C_s(2,1,0)$ site, the ESR observation¹⁷ of an "orthorhombic" site in $CaF_2:U^{3+}$ reported by Mahlab, Volterra, Low, and Yariv (MVLV) became an interesting suspect. In addition to the usual observation of the tetragonal site corresponding to the $C_{4v}(1,0,0)$ site, a group of ESR lines gave rise to a novel anisotropy pattern which MVLV attributed to the fifth-nearest-neighbor U^{3+} - F^{-} interstitial pair.²⁰ Since no trigonal sites corresponding to the presence of oxygen were observed, MVLV were probably correct in concluding that their observation was due to a new site arising from F^{-} interstitial compensation. However, as it is obvious from our present distribution calculations, the probability of finding the fifth-nearest-

²⁰ The fifth n.n. M^{3+} - F^{-} interstitial pair [$C_s(2,2,1)$] actually gives rise to a monoclinic site instead of the "orthorhombic" designation may be MVLV (Ref. 17).

neighbor pair is vanishingly small. If our calculations are at least qualitatively correct, the MVLV ESR spectral lines are most probably due to the third-nearest-neighbor $C_s(2,1,0)$ site. We shall show in detail in the following that this is indeed the case.

The effective spin Hamiltonian for the U^{3+} ion in an external magnetic field \hat{H} is

$$\mathcal{H} = \beta H_0 \left\{ g_x \cos \theta S_z + \frac{1}{2} \sin \theta [g_x \cos \phi (S_+ + S_-) - i g_y \sin \phi (S_+ - S_-)] \right\}, \quad (4)$$

where β is the Bohr magneton, g_x , g_y , and g_z are the projections of the g tensor along the x , y , z directions, respectively, H_0 is the effective magnetic field strength, θ_H the angle between the \hat{H} field and the Z axis, and ϕ_H the corresponding azimuthal angle. In C_s symmetry, Z is taken to be the axis \perp to the reflection plane, while ϕ_H is measured from the U^{3+} - F^{-} interstitial axis in the reflection plane. There are altogether 24 equivalent $C_s(2,1,0)$ sites, which are shown in Fig. 4 bisecting the edges of the six squares normal to the $[100]$, $[010]$, $[001]$, $[\bar{1}00]$, $[0\bar{1}0]$, and $[00\bar{1}]$ crystal axes. The 12 sites associated with the $[100]$, $[010]$ and $[001]$ axes are denoted by $a, a', b, b', c, c', d, d', e, e', f, f'$; respectively. Since the magnetic field is invariant upon inversion, the $[lmn]$ and $[\bar{l}\bar{m}\bar{n}]$ crystal axes are equivalent, and the 12 remaining sites associated with the $[\bar{1}00]$, $[0\bar{1}0]$, and $[00\bar{1}]$ axes are indistinguishable from the 12 above mentioned sites through an inversion of coordinates in the magnetic field. A group of sites will be magnetically equivalent if and only if their orientations with respect to the magnetic-field direction are identical in terms of the angles θ_H and ϕ_H , and of α , the angle between \hat{H} and the U^{3+} - F^{-} interstitial axis. The general features of the angular dependence of the Zeeman shifts for the twelve sites with \hat{H} rotating in the $(01\bar{1})$ plane can be ascertained as follows. When \hat{H} is in the $[100]$ direction, there are three identical groups of sites: (i) a, a', b, b' ($\alpha = 26^\circ 34'$, $\theta_H = 90^\circ$, $\phi_H = 26^\circ 34'$), (ii) c, c', e, e' ($\alpha = 63^\circ 26'$, $\theta_H = 90^\circ$, $\phi_H = 63^\circ 26'$), and (iii) d, d', f, f' ($\alpha = 90^\circ$, $\theta_H = 0^\circ$, $\phi_H = 0^\circ$). As \hat{H} is rotated away from the $[100]$ direction in the $(01\bar{1})$ plane, there are six groups of equivalent sites: a, b ; $a'b'$; c, e ; $c'e'$; d, f ; and $d'f'$, which should give rise to a maximum of six lines. With \hat{H} in the $[211]$ direction, the resulting spectrum should consist of six lines due to the six different sets of equivalent sites. (i) a, b ($\alpha = 24^\circ 06'$, $\theta_H = 65^\circ 54'$, $\phi_H = 0^\circ$); (ii) a', b' ($\alpha = 56^\circ 47'$, $\theta_H = 65^\circ 54'$, $\phi_H = 53^\circ 08'$); (iii) e, c ($\alpha = 43^\circ 05'$, $\theta_H = 65^\circ 54'$, $\phi_H = 36^\circ 52'$); (iv) e', c' ($\alpha = 90^\circ$, $\theta_H = 65^\circ 54'$, $\phi_H = 90^\circ$); (v) f, d ($\alpha = 56^\circ 47'$, $\theta_H = 35^\circ 16'$, $\phi_H = 18^\circ 26'$); and (vi) f', d' ($\alpha = 79^\circ 29'$, $\theta_H = 35^\circ 16'$, $\phi_H = 71^\circ 34'$). As \hat{H} is rotated to the $[111]$ direction, the six sets of lines merge into two due to the two sets of equivalent sites, (i) a, b, c, d, e, f ($\alpha = 39^\circ 14'$, $\theta_H = 54^\circ 44'$, $\phi_H = 18^\circ 26'$); and (ii) a', b', c', d', e', f' ($\alpha = 75^\circ 02'$, $\theta_H = 54^\circ 44'$, $\phi_H = 71^\circ 34'$). Finally, with \hat{H} in the $[011]$ direction, the spectrum should consist of four lines arising from the four different sets of equivalent sites a, b, a', b'

($\alpha=71^\circ34'$, $\theta_H=45^\circ$, $\phi_H=63^\circ26'$); c, e, c', e' ($\alpha=50^\circ46'$, $\theta_H=45^\circ$, $\phi_H=26^\circ34'$); f, d ($\alpha=18^\circ26'$, $\theta_H=90^\circ$, $\phi_H=18^\circ26'$) and f', d' ($\alpha=71^\circ34'$, $\theta_H=90^\circ$, $\phi_H=71^\circ34'$).

Since U^{3+} (f^3) is a Kramer's salt, the $S=\frac{1}{2}$ representation for the C_s spin Hamiltonian is a valid representation in view of the twofold degeneracy due to time-reversal symmetry. The parameters g_x, g_y , and g_z are evaluated from the experimental g factors reported by MVLY through the equation

$$g(\theta, \phi) = (g_x^2 \cos^2 \phi \sin^2 \theta + g_y^2 \sin^2 \phi \sin^2 \theta + g_z^2 \cos^2 \theta)^{1/2}. \quad (5)$$

For a reasonably good fit of the experimental data, the parameters g_x and g_y can be accurately determined, while g_z is a fractional number lying in the range $0 \leq g_z \leq 0.8$. The anisotropy pattern of the observed ESR lines with \hat{H} rotating in the (011) plane for $S=\frac{1}{2}$, $g_x=3.01$, $g_y=1.63$, and $g_z=0.69$ is calculated employing Eq. (4). It is plotted and compared with MVLY's data in Fig. 5. The excellent agreement between theory and the experiment leaves little doubt as to the $C_s(2,1,0)$ site origin of MVLY's spectroscopic observations.

V. DISCUSSION

The general features of the distribution curves shown in Figs. 2 and 3 appear to be in good agreement with experimental observations. If the value of $\epsilon_1 = -0.48$ eV given by Rossing¹⁹ for the association energy of the nearest neighbor $Y^{3+}-F^-$ interstitial pair is accurate, the treatment given in Sec. III should be a sound one. This experimentally determined value, however, is probably on the low side of the actual value for ϵ_1 since the observed binding energy is most likely an average binding energy of the lowest-lying bound states. If this is true, the distribution should favor the tetragonal sites even more, but the general features as presented in Figs. 2 and 3 will not be changed. We are further reassured by the fact that similar experimental determinations²¹ of ϵ_1 in (alkali halide): M^{2+} systems are seen to be in good agreement with the calculated value of Bassani and Fumi.⁵

The statement made in Sec. IV concerning the observation of cubic sites and the predicted third-nearest-neighbor $C_s(2,1,0)$ sites requires some further comment. While the so-called cubic sites must by necessity be actually lower symmetry sites due to the charge neutrality condition, whether they actually correspond to the third-nearest-neighbor C_s site depends on whether equilibrium conditions are attained or not. It has been recently determined²² that the migrational activation energy of the F^- interstitials is $34.8 \text{ kcal. mole}^{-1} = 1.51 \text{ eV}$. Assuming the frequency factors for the jump of a F^- interstitial from one interstitial position to another to be in the usual range of $10^{11}-10^{13}$, the time required

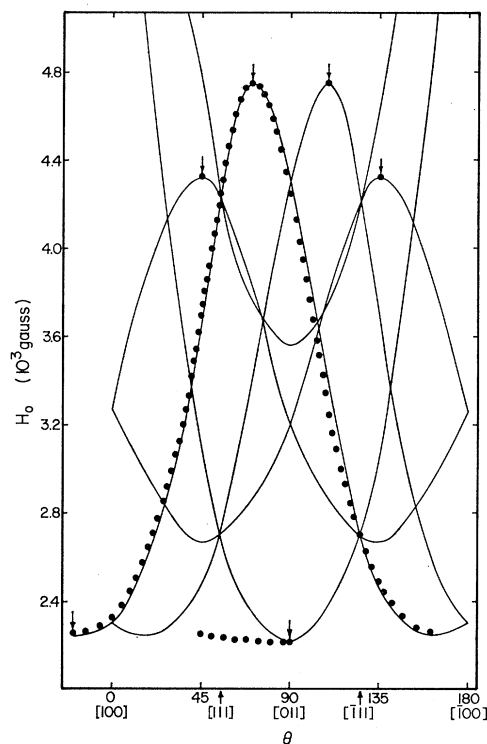


Fig. 5. Angular dependence with \hat{H} rotating in the (011) plane of 3-cm ESR lines arising from the 12 magnetically distinguishable $C_s(2,1,0)$ sites (Fig. 4) for $CaF_2:U^{3+}$. θ is the angle between \hat{H} and the [100] axis. The solid lines are theoretical calculations employing Eq. (4) with $g_x=3.01$, $g_y=1.63$, and $g_z=0.69$. The dotted lines as well as the arrows at maxima and minima of the pattern are the experimental observations made by MVLY (Ref. 17). The only and rather minor discrepancy between theory and experiment appears at the incomplete dotted line given in the vicinity of 2.3 kG between 45 and 90 deg.

for thermal equilibration of the site distribution will be on the order of $1-10^2$ sec at $T=630$ K (our temperature fit of the RPM experiment). At room temperature, however, the time required for thermal equilibration would be in the order of 10^7-10^9 years. Thus, a sample which has been annealed at high temperature and which has been rapidly quenched to room temperature will be expected to remain in a metastable equilibrium that is characteristic of the higher temperature at which it has been annealed. In this case, the more distant sites will certainly be of prominence. The ideas outlined above are in agreement with the results of Friedman and Low's annealing and quenching experiments,²³ and may well be the underlying reasons for much of the conflicting results obtained when the crystal preparation techniques are not carefully reproducible.

In earlier work^{22,24} on the reduction of trivalent rare earth ions to the divalent state in alkaline earth halides, the prevailing assumption was that the impurity cation

²³ E. Friedman and W. Low, *J. Chem. Phys.* **33**, 1275 (1960).

²¹ A. B. Lidiard, *Phys. Rev.* **94**, 29 (1954); H. W. Etzel and R. J. Maurer, *J. Chem. Phys.* **18**, 1003 (1950).

²² F. K. Fong and M. A. Hiller, *J. Phys. Chem.* **71**, 2854 (1967).

²⁴ F. K. Fong, in *Progress in Solid State Chemistry*, edited by H. Reiss (Pergamon Press, Inc., New York, 1966), Vol. III, Chap. 4; F. K. Fong and J. B. Fenn, Jr. (to be published).

was either in close association with the compensation resulting in the removal of the inversion center of the impurity site or that the impurity cation is essentially in a cubic site beyond any significant influence of the distant compensation. In view of the present investigation, some of the observations unexplainable in terms of the dissociation-association hypothesis can now be reexamined. For example, the glow curve observed²⁴ when Dy²⁺ ions in CaF₂ produced by γ radiation are oxidized to the trivalent state by thermal excitation is characterized by several prominent peaks. If only the nonlocal "cubic" sites are reduced, only one glow peak can be expected.²⁴ In view of our present discussion, the multi-peaked glow curve of the Dy²⁺ \rightarrow Dy³⁺ + e^- process in CaF₂ can be readily accounted for in terms of the Maxwell-Boltzmann distribution of site symmetries depicted in Sec. III.

Finally, a comment should be made on the effect of the relative sizes of the trivalent cation and the host

ion which it replaces. In Table I, we detect a trend in which the tetragonal site and the trigonal site reverse in prominence as the host ion increases from Ca²⁺ to Ba²⁺. A qualitative argument may be made on the basis of the collapse of the 8 nearest-neighbor fluoride ions about the trivalent cation as it replaces the increasingly larger divalent cation. This will have the net effect of increasing the shielding between the trivalent cation and the (1,0,0) F⁻ interstitial thus reducing ϵ_1 . ϵ_2 on the other hand would increase as the F⁻ interstitial at (1,1,1) moves closer to the trivalent cation because of the inward displacement of the nearest neighbor fluoride ions, thus accounting for the observed changes in the relative abundance of the first two n.n. sites. A more quantitative approach is now being attempted through an extension of the lattice theory calculations of Franklin²⁵ to a calculation of ϵ_1 and ϵ_2 for the various (alkaline-earth fluoride):M³⁺ systems.

²⁵ A. D. Franklin, J. Phys. Chem. Solids 29, 823 (1968).

Effective Hamiltonian for Non-Kramers Doublets

SHŪKŌ WASHIMIYA

Broadcasting Science Research Laboratories of Nippon Hōsō Kyōkai, Kinuta, Setagaya-Ku, Tokyo, Japan

AND

KOHSEI SHINAGAWA*

Department of Physics, Tokyo Institute of Technology, Ookayama, Meguro-Ku, Tokyo, Japan

AND

SATORU SUGANO*

Institute for Solid State Physics, University of Tokyo, Azabu, Minato-Ku, Tokyo, Japan

(Received 22 August 1969)

A method of irreducible tensor operators is described for constructing effective Hamiltonians for non-Kramers doublets. It is pointed out that this method is superior in several points to other methods. The exact effective Hamiltonians for all the non-Kramers doublets in 32 point groups are tabulated. These Hamiltonians involve the effects of magnetic and electric fields up to the second order as well as those of the hyperfine interactions. The interaction of nuclear spins with a magnetic field is taken into account to the first order. Finally, selection rules for paraelectric and paramagnetic resonances are derived by use of the effective Hamiltonians for all the non-Kramers doublets.

I. INTRODUCTION

THE doubly degenerate (not accidentally degenerate) levels of molecular systems with an even number of electrons are called non-Kramers doublets. They belong to the doubly degenerate irreducible representations of the point groups (the single groups). The purpose of the present paper is to describe a clear method of constructing an effective Hamiltonian for non-Kramers doublets and to list all the effective Hamiltonians which may be used in the analysis of

electron paramagnetic resonance and optical experiments for non-Kramers doublets. In our treatment, the Jahn-Teller effect will be entirely ignored. This effect can be operative in non-Kramers doublets, but it would not be so important in the 4f-electron systems on which experimental work has been concentrated.

So far, several studies have been done on the spin Hamiltonian for non-Kramers doublets. Bleaney and Scovil¹ first introduced a spin Hamiltonian

$$3\mathcal{C} = g_{11}\beta H_z S_z + A_{11}I_z S_z + \Delta_x S_x + \Delta_y S_y, \quad (1)$$

* Work partly supported by the Broadcasting Science Research Laboratories of Nippon Hōsō Kyōkai.

¹ B. Bleaney and H. E. D. Scovil, Phil. Mag. 43, 999 (1952).